```
begin
    using Pkg; Pkg.activate(".")
    using Images, FileIO, PlutoUI
end
```

# Table of Contents



- `TableOfContents()`

# Abstract

# 1. Introduction

# 2. Method

## 2.1 - Simulation

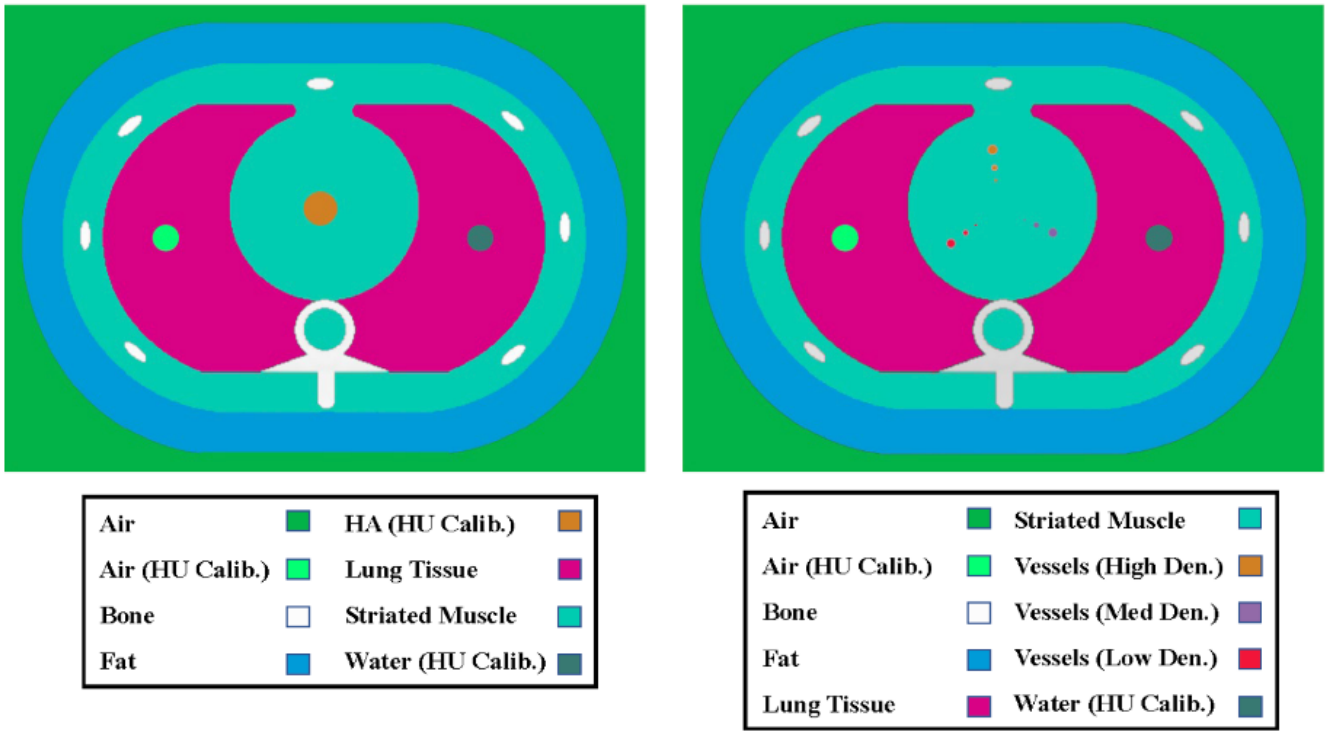


Fig. 1 Shows a sketch of the simulated phantom with the colors highlighting the different materials in the simulated phantoms.

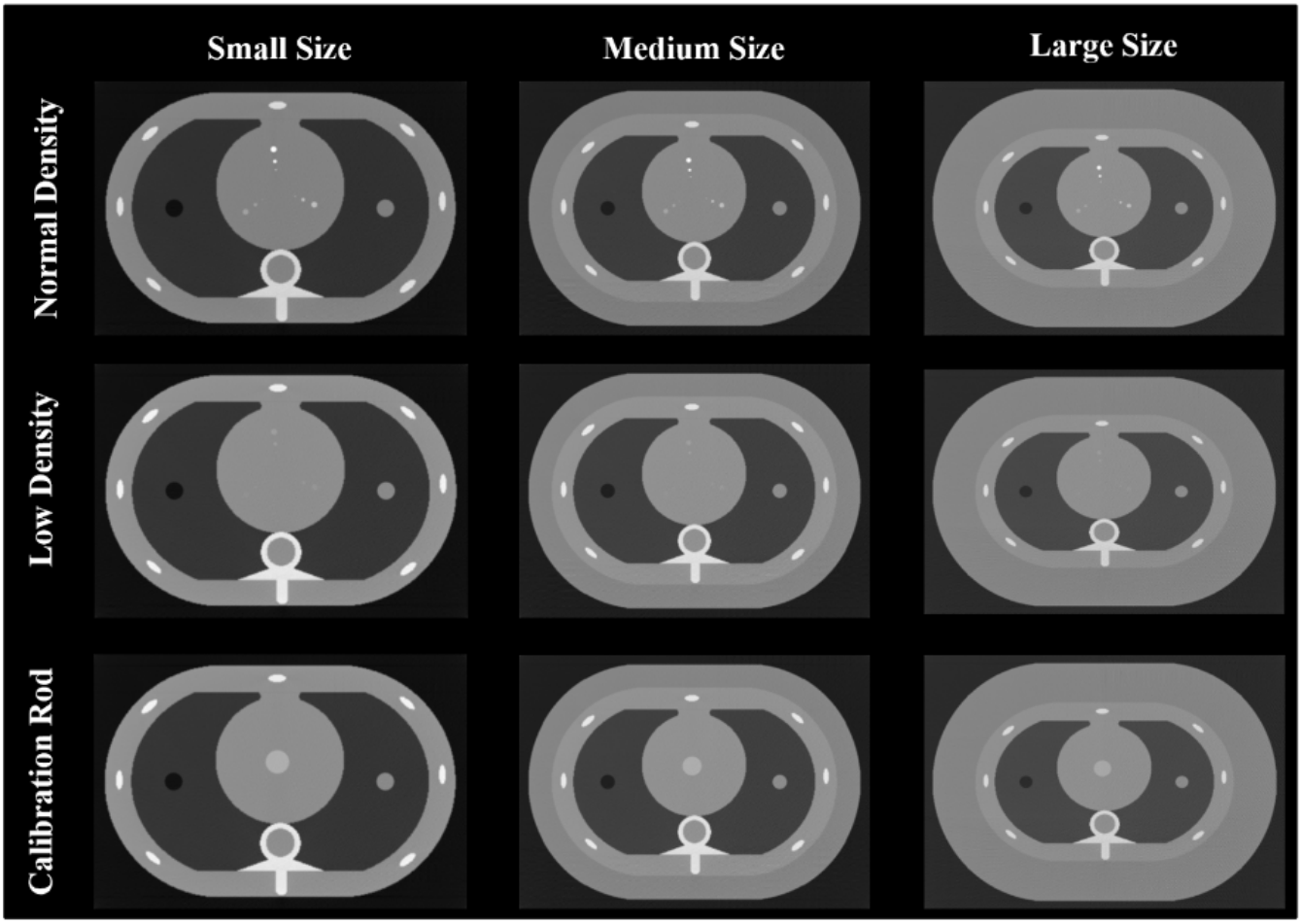


Fig. 2 Shows simulated phantom images of different phantom sizes and densities

### 2.1.1 - Motion Blurring

## 2.2 - Physical Phantom

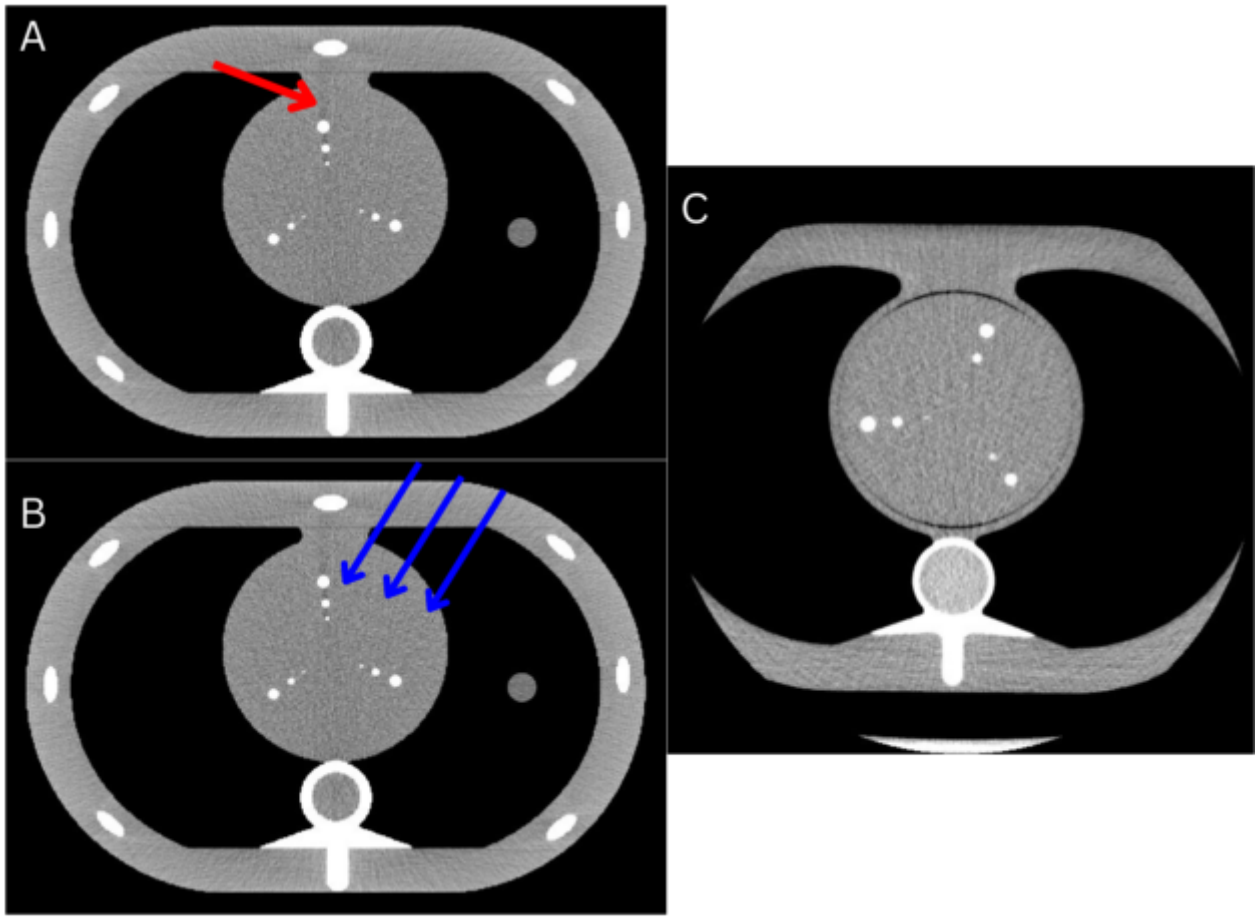


Fig 3. Shows axial slice views of a small simulated phantom with a tube voltage of 120 kV, with (B) and without (A) simulated motion. (C) Shows an axial slice view of a physical QRM Thorax Phantom with a Cardio Calcification Insert. The red arrow shows simulated beam hardening artifact and the blue arrows show simulated streakng artifact.

## 2.3 - Agatston Scoring

## 2.4 Integrated Calcium Mass

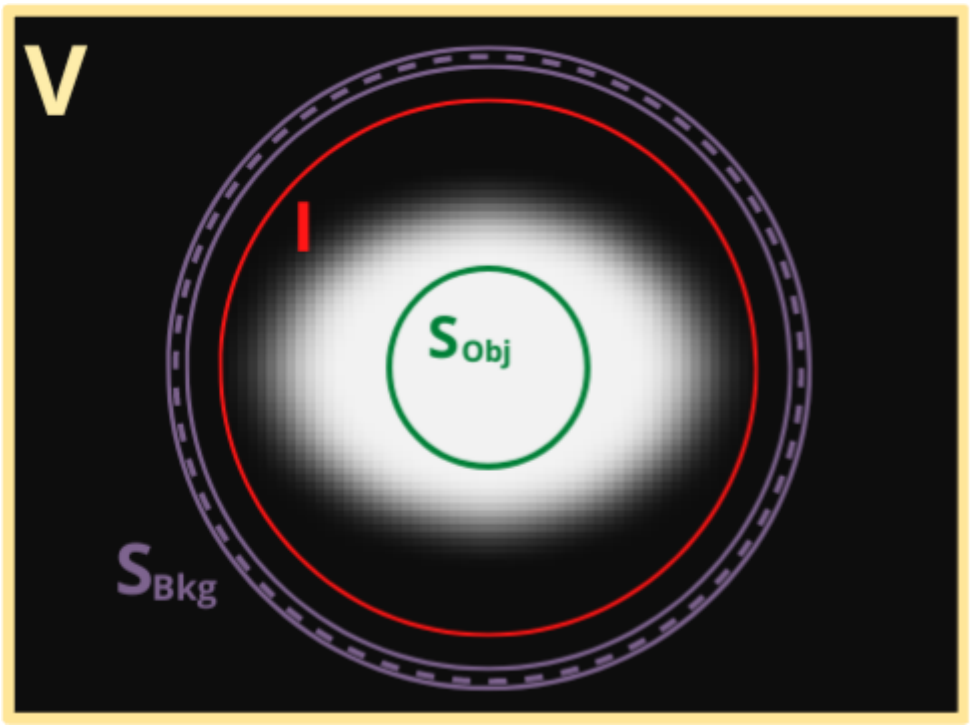


Fig 4. Shows a simulated vessel lumen with ROIs for calcium measurement where the central ROI that yields $S_{Obj}$ and the background ROI that yields $S_{Bkg}$ are unaffected by partial volume effect while the object ROI used to calculate $I$ is affected by partial volume effect.

### 2.4.1 - Calibration

## 2.5 - Volume Fraction Mass

## 2.6 - Statistical Analysis

# 3. Results

## 3.1 - Stationary

### 3.1.1 - Accuracy

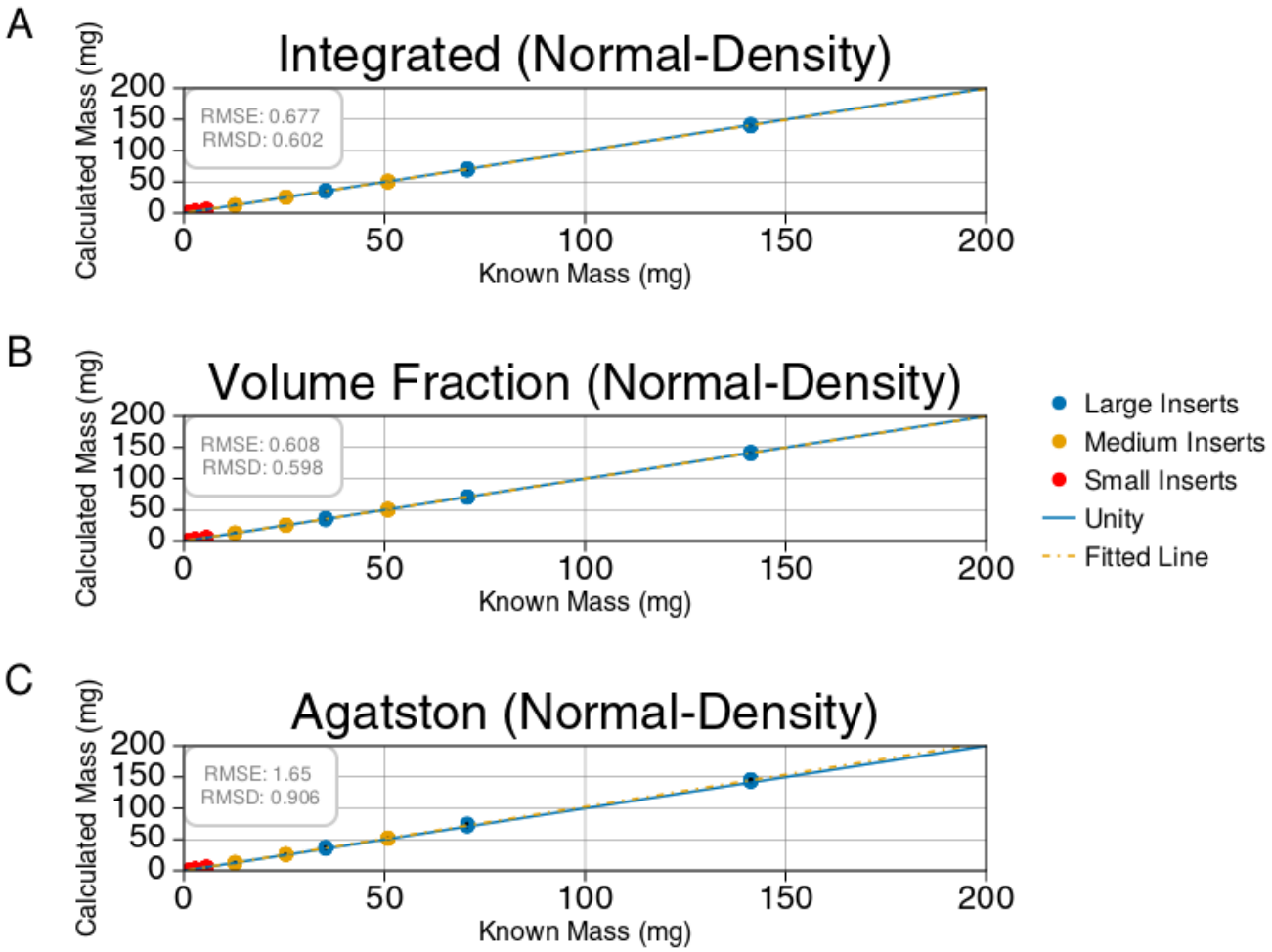


Fig. 5 Shows the linear regression analysis comparing measured calcium to the known calcium for the normal density (200, 400, 800 mg/ cm3) stationary phantoms. Fig 5A shows the results of integrated calcium mass. Fig 5B shows the results of the volume fraction method. Fig 5C shows the results of Agatston mass scoring. The best fit line along with the root mean squared error and root mean squared deviation values are shown in each plot.

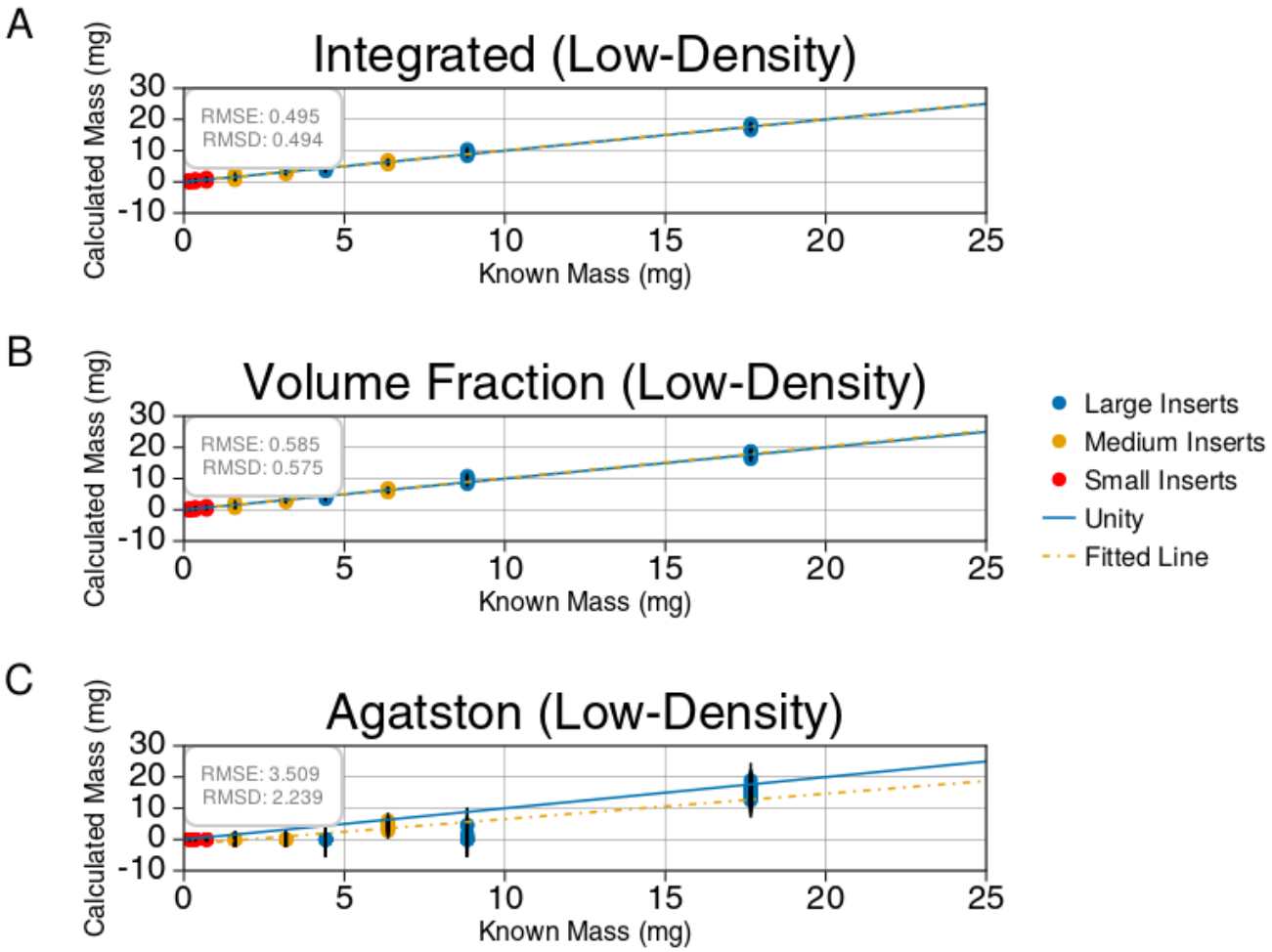


Fig. 6 Shows the linear regression analysis comparing measured calcium to the known calcium for the low-density (25, 50, 100 mg/ cm3) stationary phantoms. Fig 6A shows the results of integrated calcium mass. Fig 6B shows the results of the volume fraction method. Fig 6C shows the results of Agatston mass scoring. The best fit line, along with the root mean squared error and root mean squared deviation values are shown in each plot.

## 3.1.2 - Reproducibility

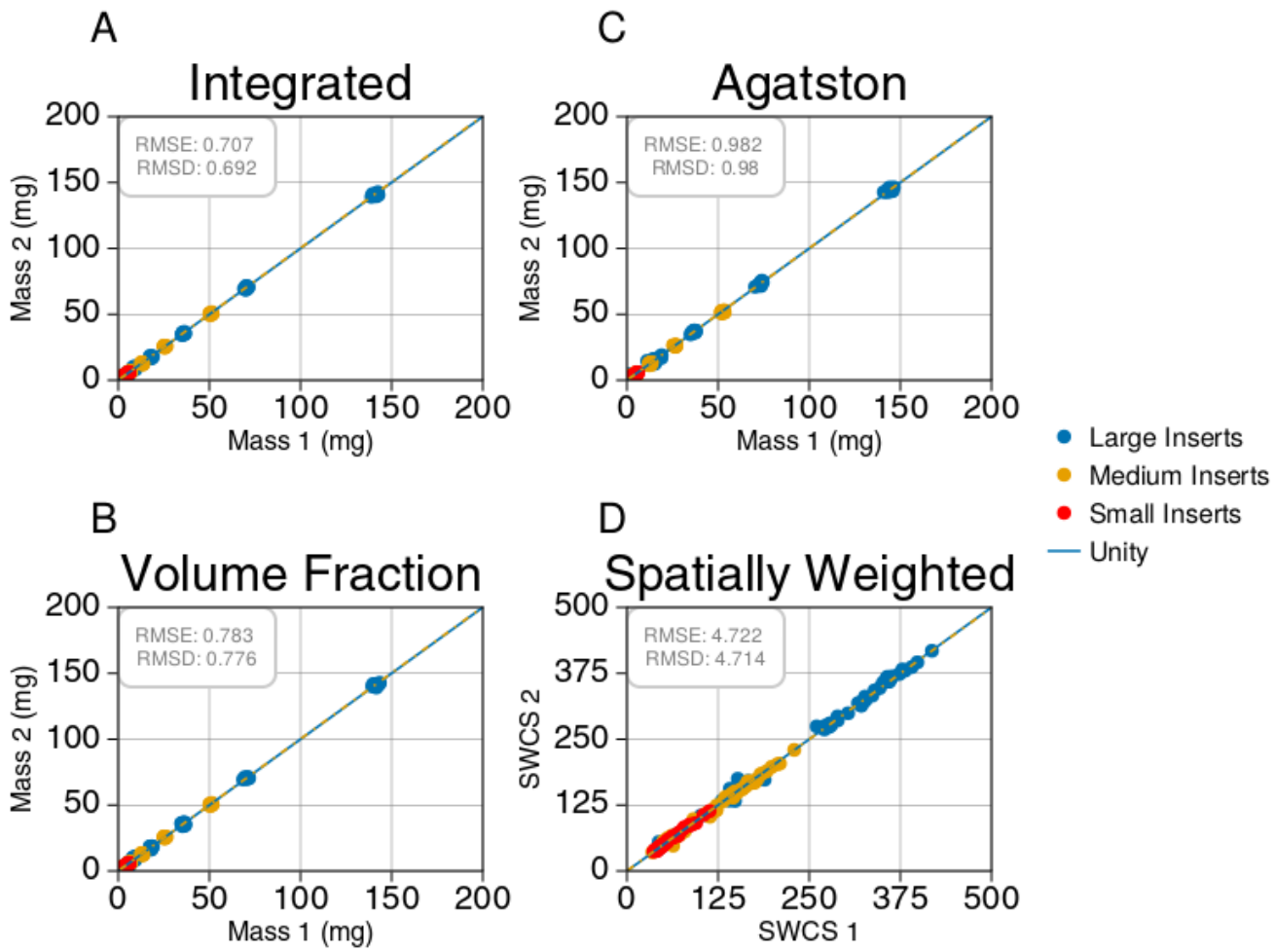


Fig. 7 Shows reproducibility measurements for all four scoring techniques on the stationary phantoms. The measurements from the first set of images were plotted against the second set of images for each technique. Integrated mass (A), Volume fraction (B), Agatston mass scoring (C), and spatially weighted calcium scoring (D) are shown along with the root mean squared error and root mean squared deviation values.

## 3.1.3 - Sensitivity and Specificity

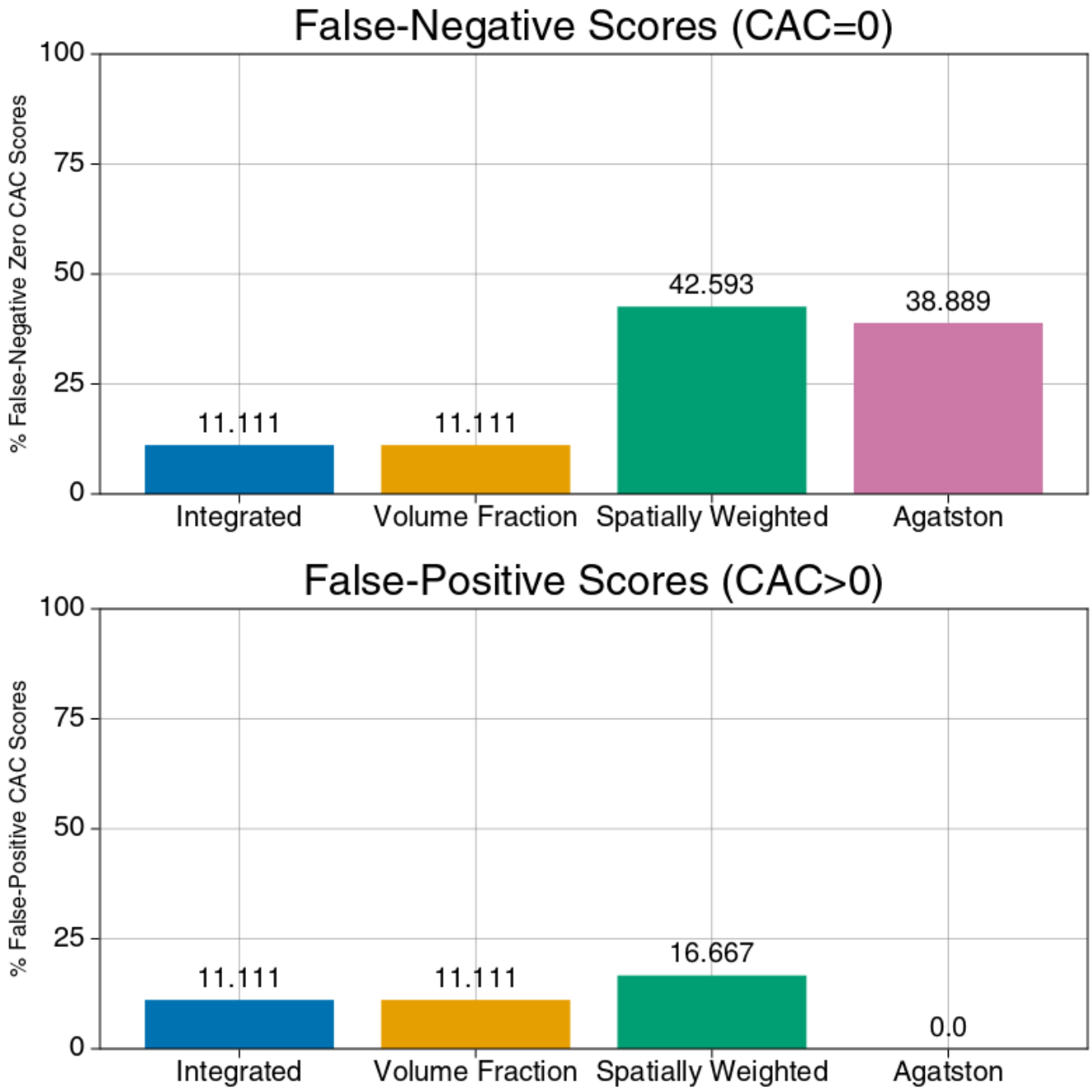


Fig 8. Shows the percentage of false-negative (CAC=0) and false-positive (CAC>0) scores for a region of pure background on the stationary phantoms.

# 3.2 - Motion

## 3.2.1 - Accuracy

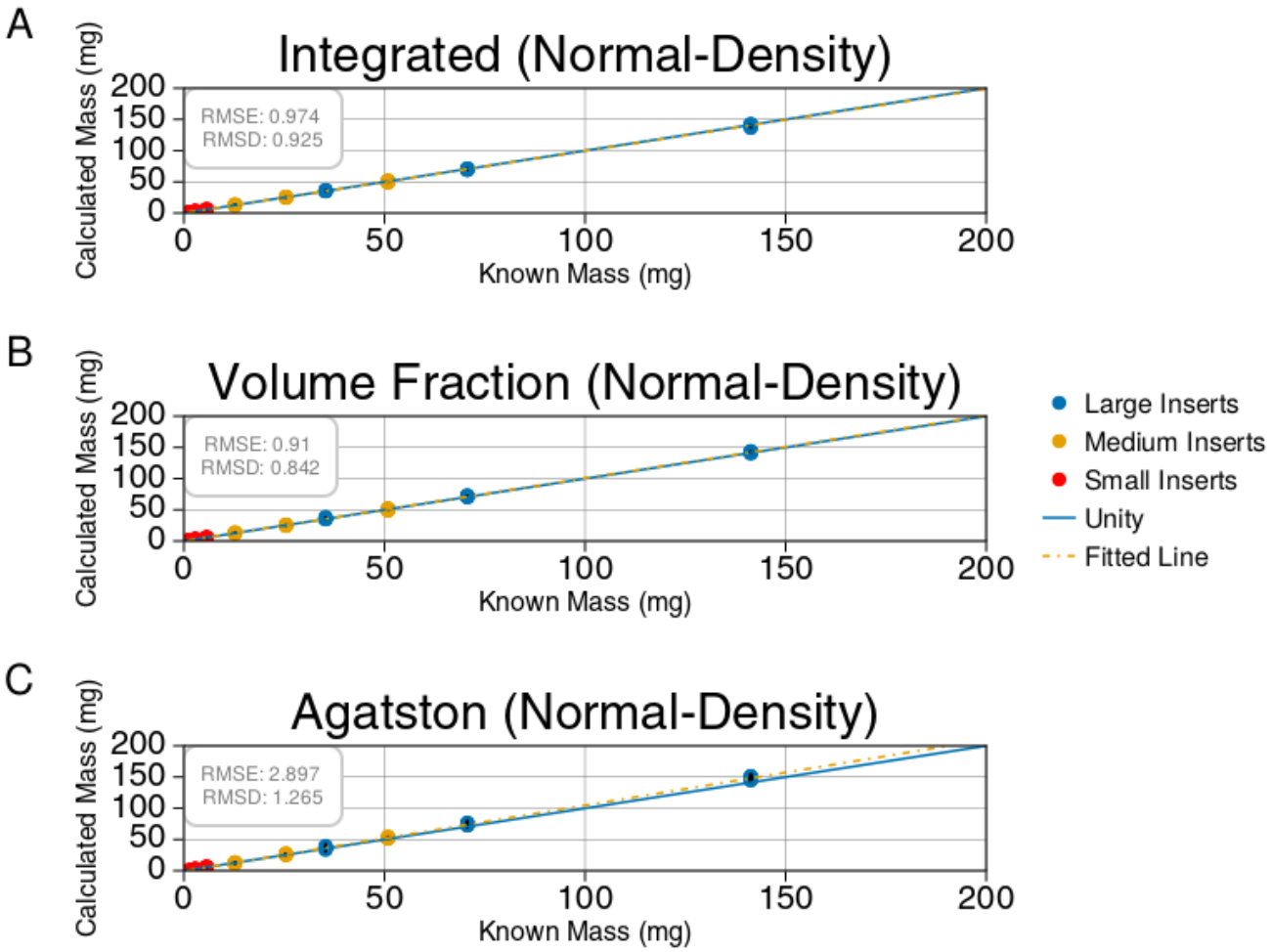


Fig. 9 Shows the linear regression analysis comparing measured calcium to the known calcium for the normal density (200, 400, 800 mg/ cm3) motion-affected phantoms. Fig 9A shows the results of integrated calcium mass. Fig 9B shows the results of the volume fraction method. Fig 9C shows the results of Agatston mass scoring. The best fit line, along with the root mean squared error and root mean squared deviation values, are shown in each plot.

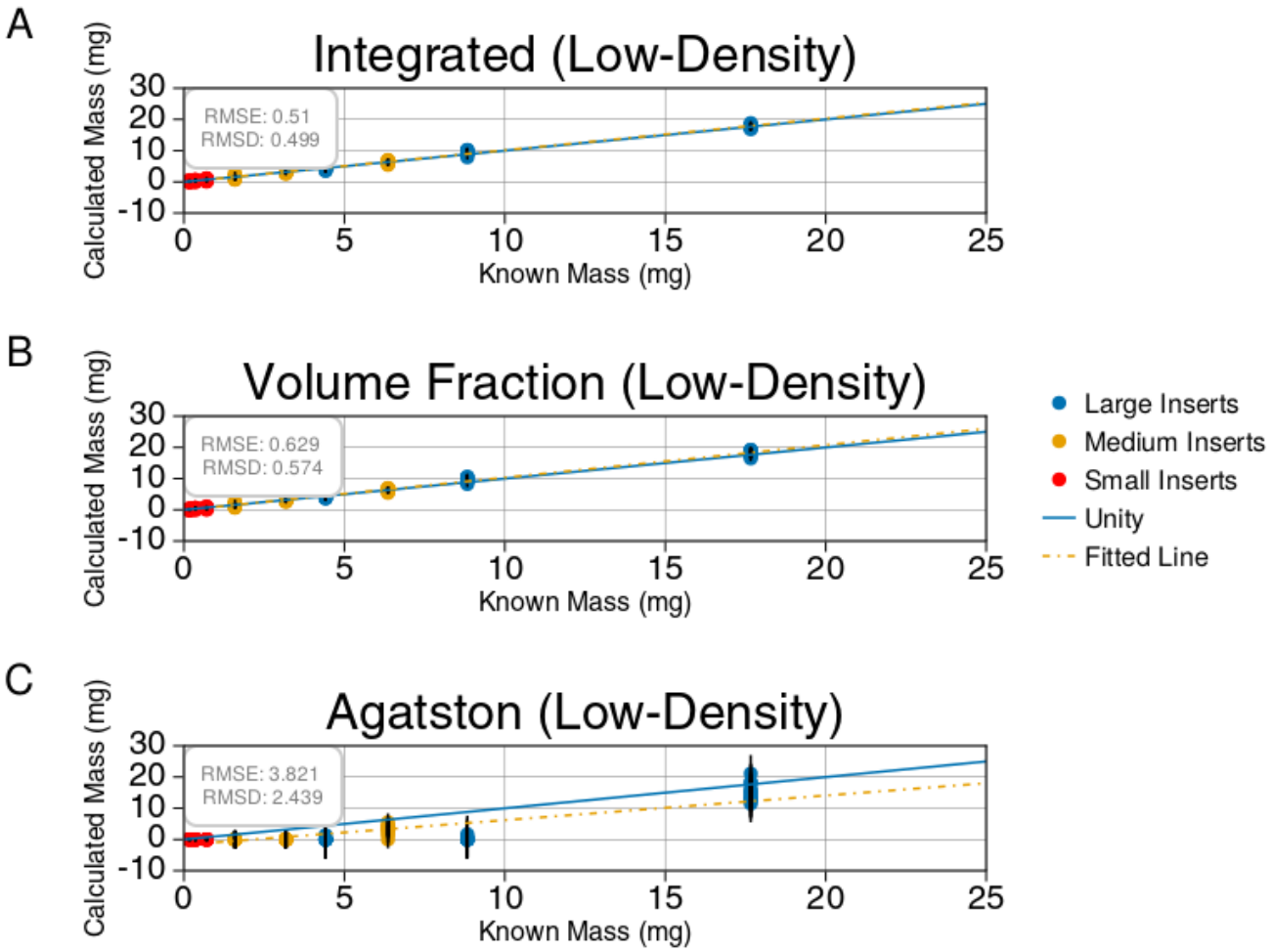


Fig. 10 Shows the linear regression analysis comparing measured calcium to the known calcium for the low-density (25, 50, 100 mg/ cm3) motion-affected phantoms. Fig 10A shows the results of integrated calcium mass. Fig 10B shows the results of the volume fraction method. Fig 10C shows the results of Agatston mass scoring. The best fit line, along with the root mean squared error and root mean squared deviation values, are shown in each plot.

## 3.1.2 - Reproducibility

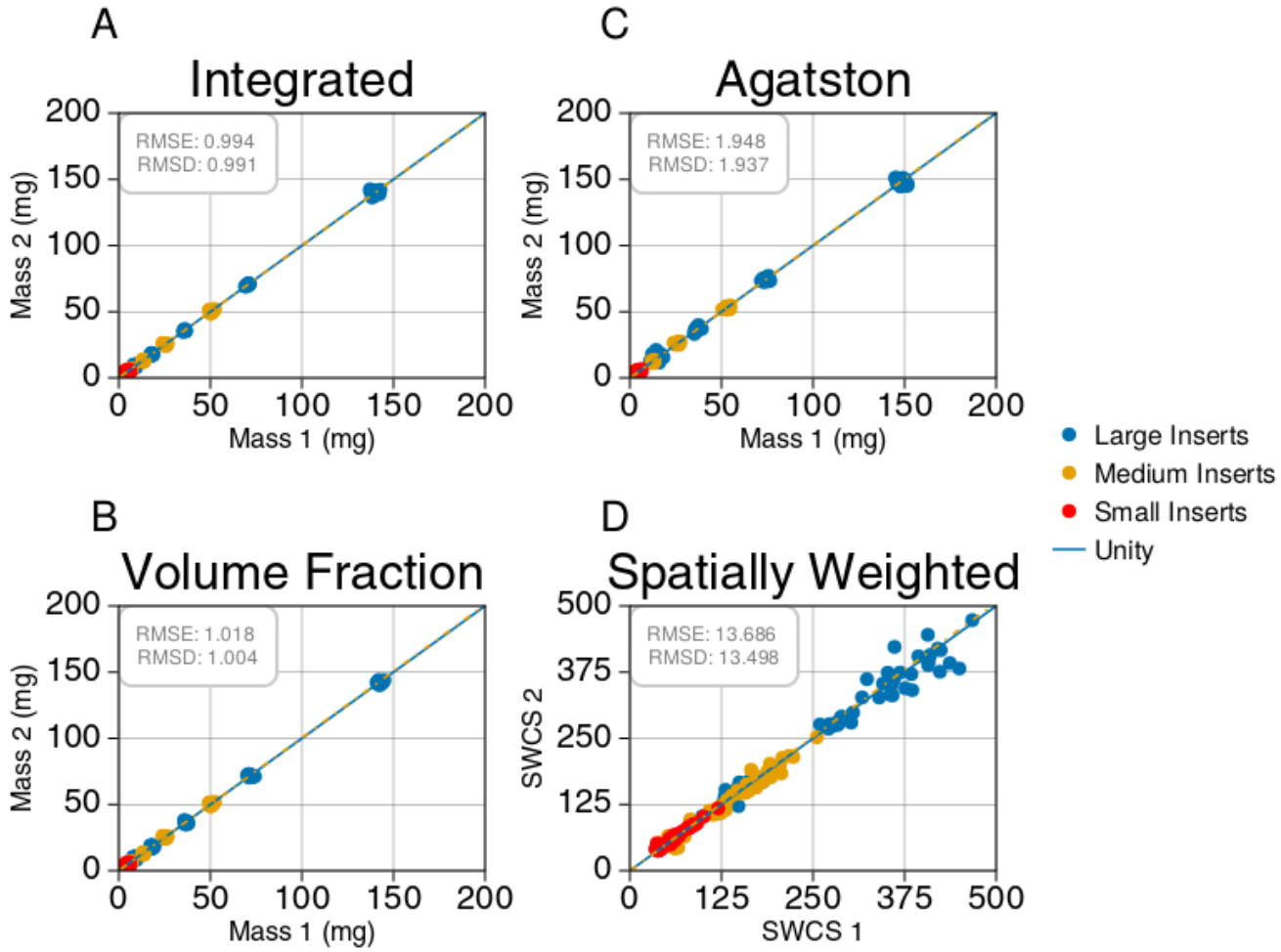


Fig. 11 Shows reproducibility measurements for all four scoring techniques on the motion-affected phantoms. The measurements from the first set of images were plotted against the second set of images for each technique. Integrated mass (A), Volume fraction (B), Agatston mass scoring (C), and spatially weighted calcium scoring (D) are shown along with the root mean squared error and root mean squared deviation values.

## 3.1.3 - Sensitivity and Specificity

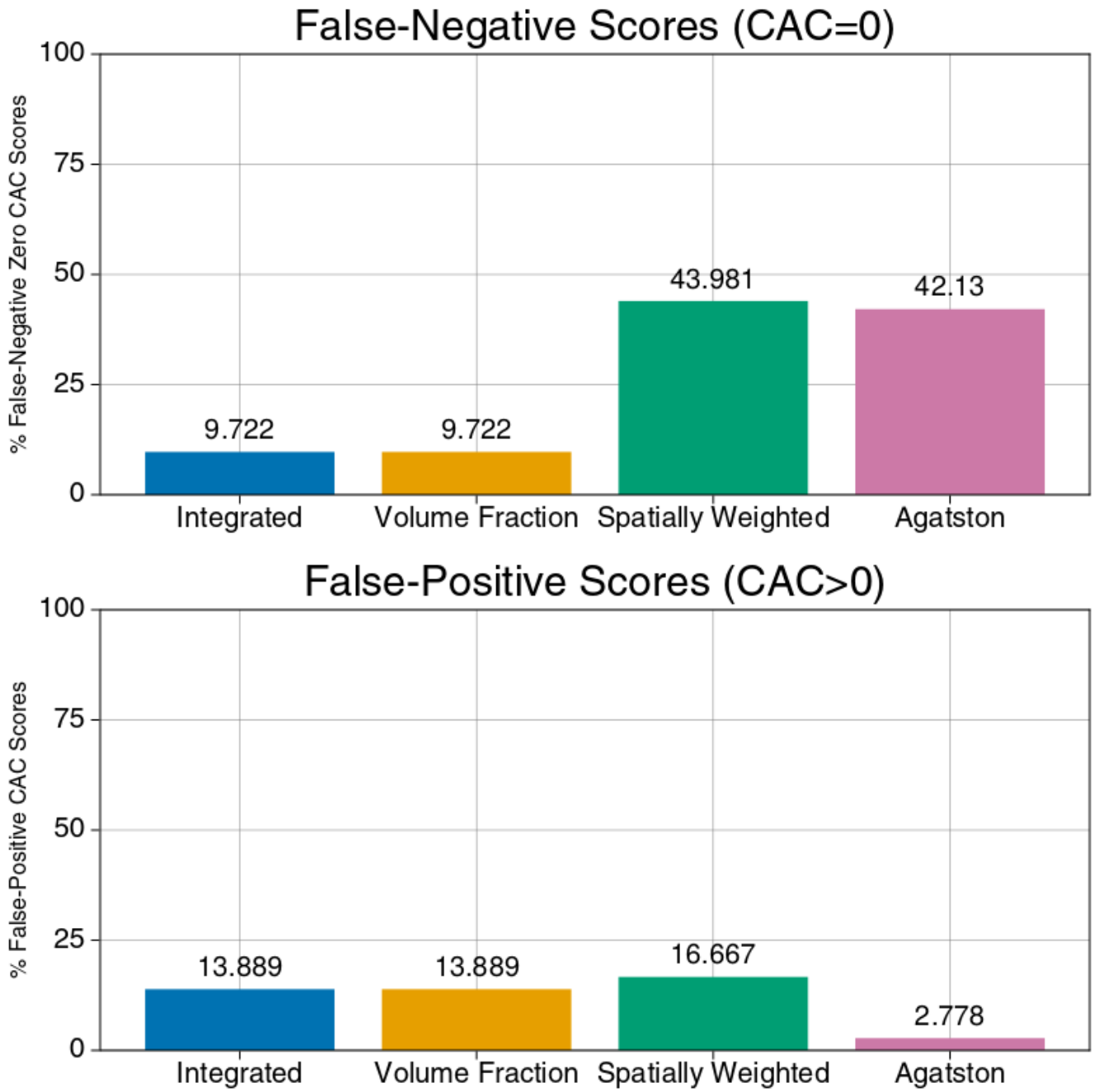


Fig 12. Shows the percentage of false-negative (CAC=0) and false-positive (CAC>0) scores for a region of pure background on the motion-affected phantoms.

# 3.2 - Physical Phantom

## 3.1.1 - Accuracy

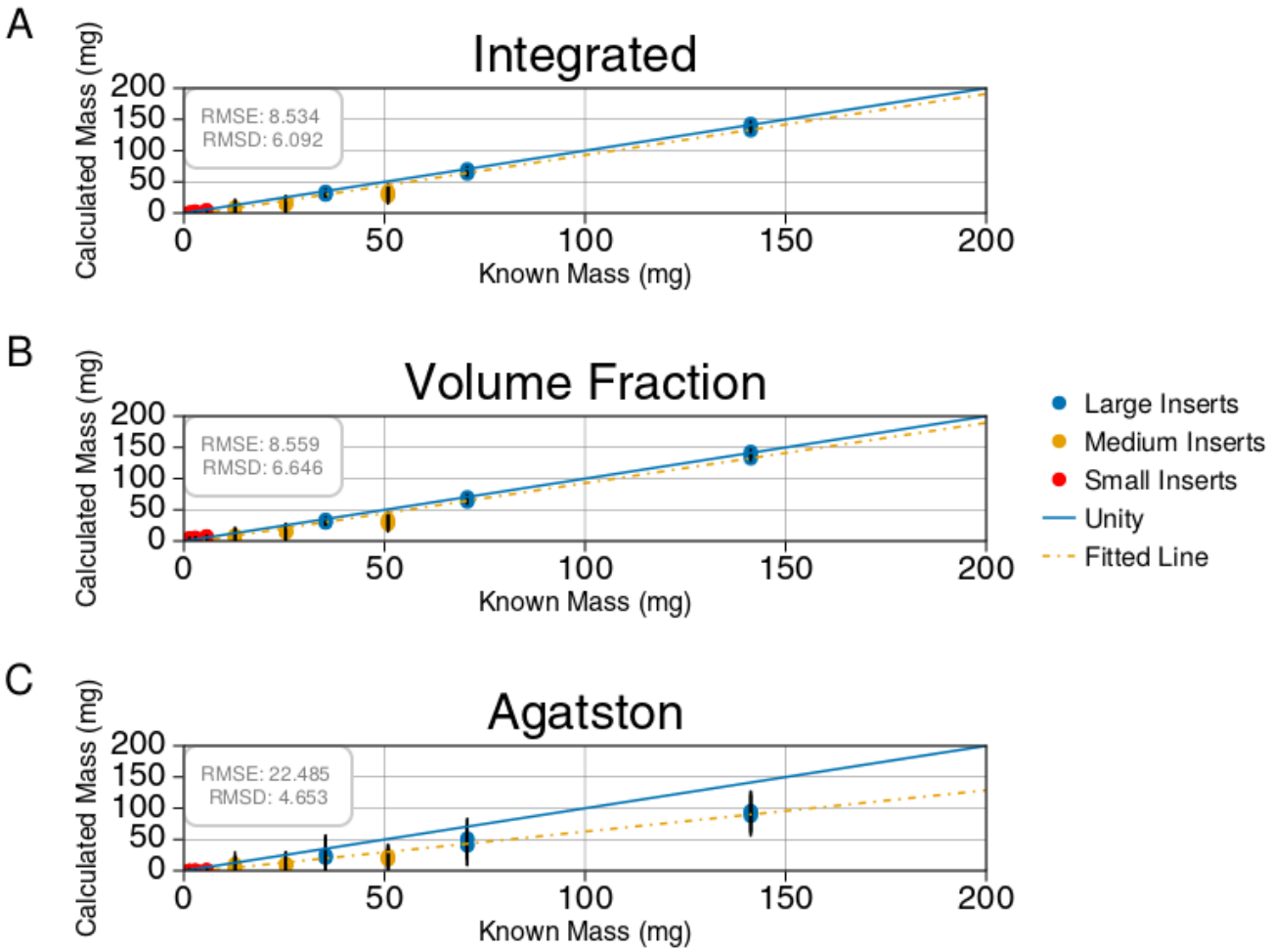


Fig. 13 Shows the linear regression analysis comparing measured calcium to the known calcium for the normal density (200, 400, 800 mg/ cm3) physical phantom scans. Fig 13A shows the results of integrated calcium mass. Fig 13B shows the results of the volume fraction method. Fig 13C shows the results of Agatston mass scoring. The best fit line, along with the root mean squared error and root mean squared deviation values, are shown in each plot.

## 3.1.2 - Reproducibility

*Note: The reproducibility results show a lower RMSE and RMSD for Agatston compared to Integrated and Volume Fraction. This is misleading because Agatston underestimates the mass by almost 50%, so the reproducibility comparison between smaller numbers is of course going to result in a smaller RMSE/D than Integrated/Volume Fraction techniques.*

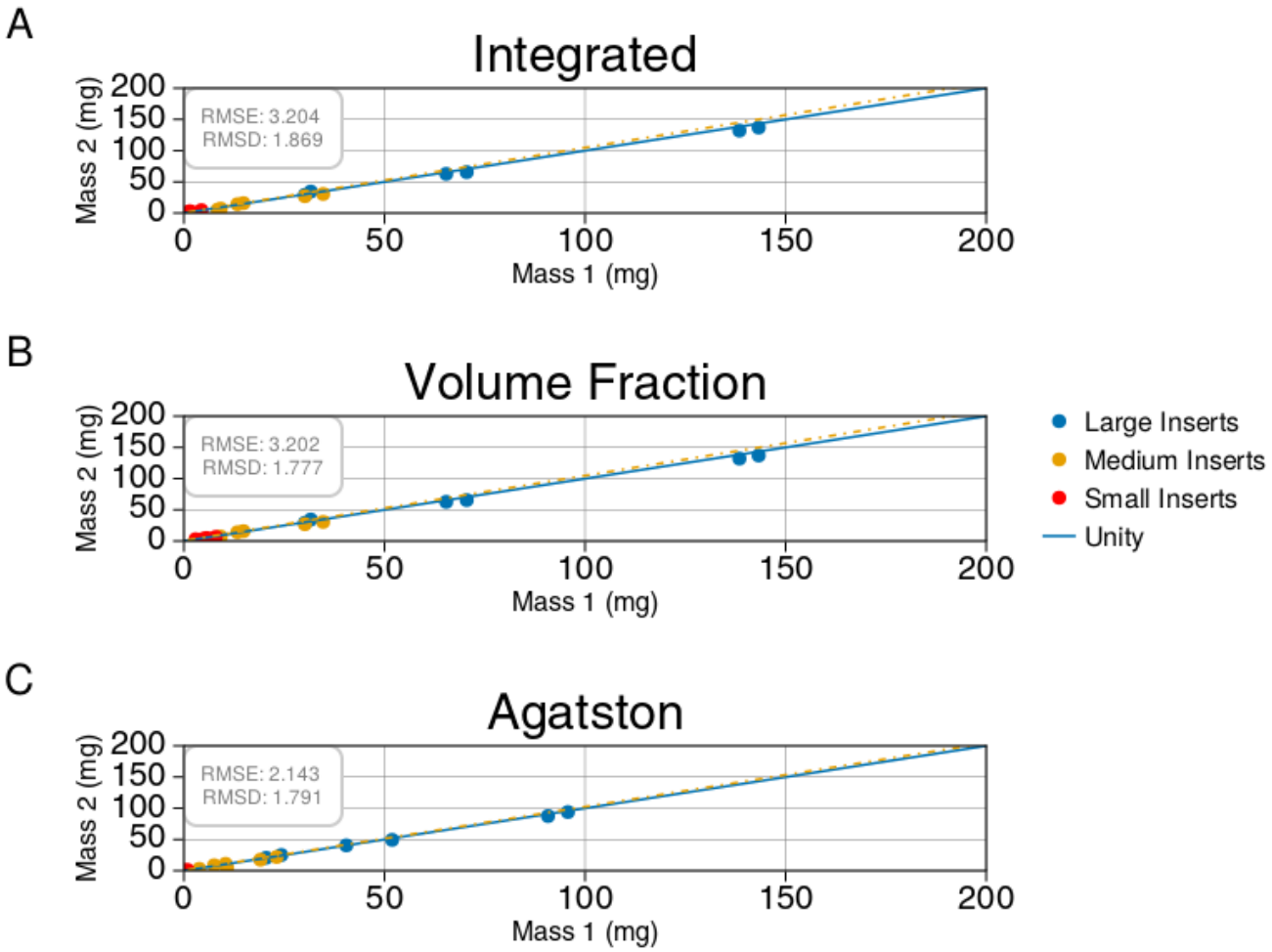


Fig. 14 Shows reproducibility measurements on the physical phantom scans. Measurements from two scans were plotted against a second set of measurements from two different scans at different angles. Integrated mass (A), Volume fraction (B), Agatston mass scoring (C) are shown along with the root mean squared error and root mean squared deviation values.

## 3.1.3 - Sensitivity and Specificity

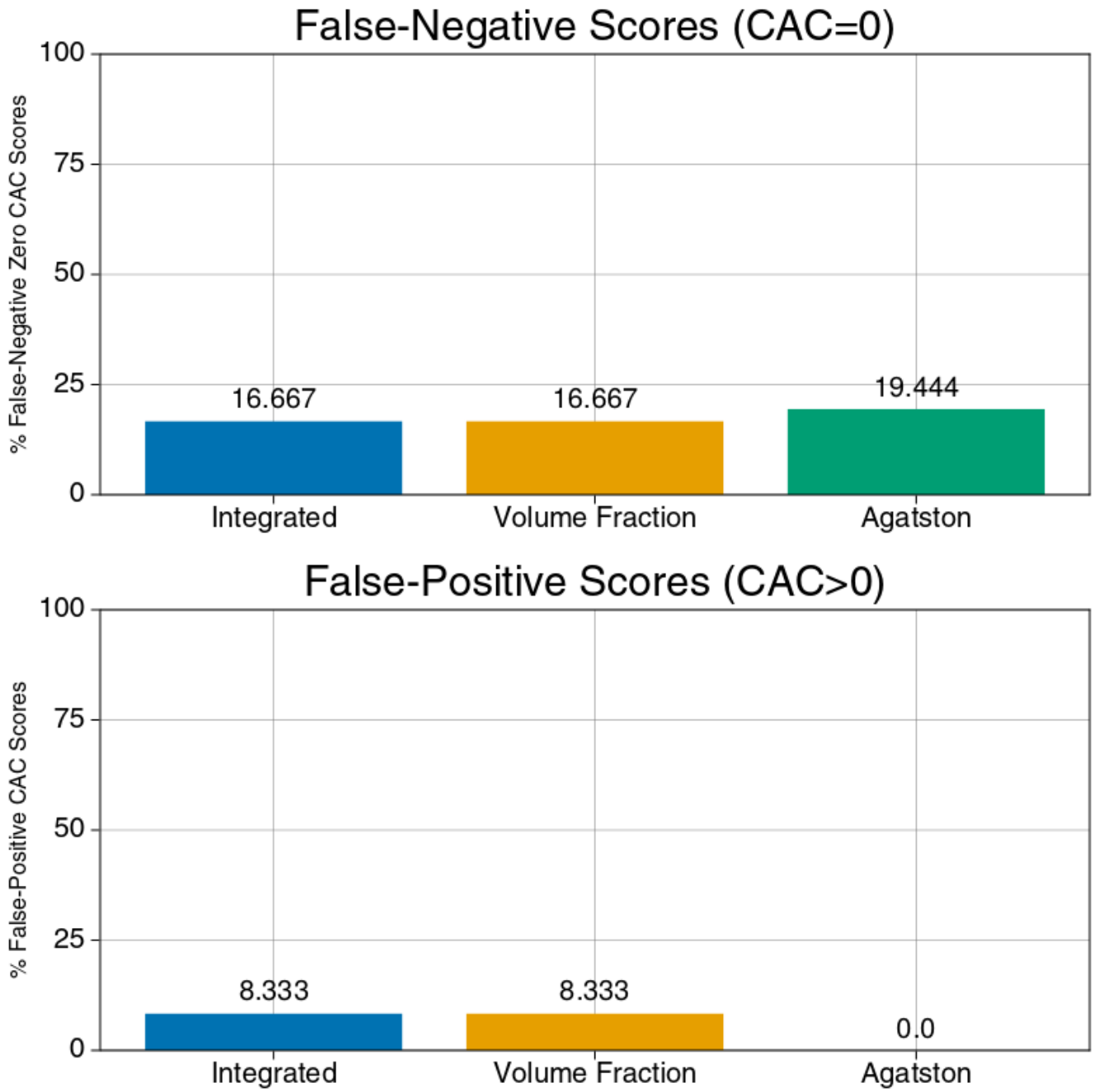


Fig 15. Shows the percentage of false-negative (CAC=0) and false-positive (CAC>0) scores for a region of pure background on the motion-affected phantoms.

# 4. Discussion

# 5. Conclusion

# Acknowledgements

# References